Energy Conversion and Management 293 (2023) 117518

Contents lists available at ScienceDirect

Energy Conversion and Management

journal homepage: www.elsevier.com/locate/enconman

A novel electrochemical system with adiabatic pre-charging and pre-discharging processes for efficient refrigeration

Bo Chen [a], Julian Gonzalez-Ayala [b,c], A. Calvo Hernández [c,d], Rongxiang Luo [a], Hanxin Yang [a], Juncheng Guo [a]

[a] College of Physics and Information Engineering, Fuzhou University, Fuzhou 350116, People's Republic of China
[b] Escuela Politécnica de Avila, Universidad de Salamanca, Spain
[c] Departamento de Física Aplicada, Universidad de Salamanca, 37008 Salamanca, Spain
[d] Instituto Universitario de Física Fundamental y Matemáticas (IUFFyM), Universidad de Salamanca, 37008 Salamanca, Spain

ARTICLE INFO

Keywords:
Thermally regenerative electrochemical refrigerator
Heating by discharging
Cooling by charging
Electrochemical counterpart
Adiabatic pre-charging process
Adiabatic pre-discharging process

ABSTRACT

The extraordinary thermal-to-electricity conversion efficiency of thermally regenerative electrochemical cycle triggers interest in its reverse counterpart, namely thermally regenerative electrochemical refrigerator (TRER), a promising alternative to conventional cooling devices. Nevertheless, due to three fundamental obstacles, the practically feasible TRER model is still absent, which hinders the development of follow-up research. To break this bottleneck, heating by discharging and cooling by charging effects are innovatively utilized to construct TRER models where the electrochemical counterparts of traditional adiabatic compression and expansion processes, namely adiabatic pre-charging and pre-discharging processes, are proposed and introduced. Significantly, the maximum coefficient of performance (COP) and the COP at maximum cooling power are predicted to achieve up to 40% and 5% of Carnot COP, respectively for the given values of parameters. Moreover, the great potential for efficient refrigeration is highlighted by comparing the obtained results with various refrigeration systems. This work lays the foundation for further experimental investigations and opens a new avenue for constructing other novel electrochemical cycles.

1. Introduction

The widely used vapor-compression refrigeration systems consume approximately 10% of the electricity generated worldwide [1] and represent a significant fraction of the gas emission contributing to ozone depletion and global warming [2], which fuels the global energy crisis and environmental problems. Regarding this concern, various novel refrigeration technologies, such as adsorption refrigeration [3], thermoelectric cooling [4,5], magnetic refrigeration [6], barocaloric refrigeration [7], thermal Brownian refrigeration [8], thermionic refrigeration [9], and energy selective electron cooling [10] have been continually proposed and extensively studied. Although the fundamental understanding and practical improvement have been remarkable, these alternatives are still facing the challenges in efficiency, cost, and system complexity to compete with conventional refrigerators. Consequently, it is of great significance to further explore better refrigeration technologies.

Recently, based on the thermogalvanic effect and the temperature dependence of electrode potential, a novel thermally regenerative electrochemical cycle (TREC) employing highly reversible electrode materials with low polarization has been put forward for efficiently harvesting low-grade thermal energy [11]. Notably, a high thermal-to-electricity conversion efficiency of 5.7%, corresponding to approximately 38% of Carnot efficiency, is achieved when the system is operated between 10 and 60 °C [11]. The extraordinary conversion efficiency in both high and low temperature applications, along with the merits of reliability, quietness, and environmental friendliness, has triggered the heated researches about TERC once again. Considerable efforts have been dedicated to exploring materials with larger temperature coefficient [12–15] and lower resistance [16]. To minimize costs, simplify the system, and achieve continuous power output, membrane-free [17], charging-free [18,19], and continuous [19–24] TREC systems have been proposed, respectively. Besides, several objective functions [24,25] have been adopted to provide more comprehensive operation criteria. In addition, various electrochemical cycle configurations, such as electrochemical Carnot cycle [26] and electrochemical Brayton cycle [27], have been presented, analyzed, and compared. Moreover, with the superiority of wide adaptability, various TREC-based hybrid systems [28–30] have been presented and investigated.

E-mail address: junchengguo@qq.com (J. Guo).

https://doi.org/10.1016/j.enconman.2023.117518
Received 23 June 2023; Received in revised form 26 July 2023; Accepted 7 August 2023

Nomenclature

Latin letters

C_p	heat capacity (J/K)
C_q	charge capacity (C)
c_p	specific heat capacity ($J/(K\cdot kg)$)
c_q	specific charge capacity (C/kg)
F	Faraday constant (C/mol)
I	electric current (A)
K	heat transfer coefficient (W/K)
K_L	heat leakage coefficient (W/K)
M	number of cells in one cell pack
N	total number of cells adopted
n_e	number of electrons transferred
P	power input (W)
Q	heat (J)
Q_{ad}	additional heat required to attain objective temperatures (J)
Q_e	electrode charge (C)
Q_L	heat leakage (J)
Q_{re}	regeneration heat (J)
R	cooling power (W)
R_{int}	internal resistance (Ω)
S	entropy (J/K)
s	partial molar entropy ($J/(K\cdot mol)$)
T	temperature (K)
$T_c^{'}$	cell temperature after the cooling regeneration process (K)
$T_h^{'}$	cell temperature after the heating regeneration process (K)
t	time (s)
V	voltage (V)
v	stoichiometric number

Greek letters

α_c	temperature coefficient (V/K)
ε	coefficient of performance
ε_{Car}	Carnot coefficient of performance
ε_{rep}	reported coefficient of performance
η	efficiency
η_{re}	regenerative efficiency
τ	overall cycle time (s)

Subscript

C	low temperature heat source
c	low cell temperature in the isothermal process
ch	charging process
dis	discharging process
H	high temperature heat source
h	high cell temperature in the isothermal process
j	the jth chemical involved
max	maximum
oc	open circuit state
pch	pre-charging process
$pdis$	pre-discharging process
Rm	maximum cooling power state
εm	maximum coefficient of performance sate

Abbreviations

COP	coefficient of performance
Cu	copper
Cu2+	cupric
CuHCF	copper hexacyanoferrate
Gd	gadolinium
HC	high-current operating mode
LC	low-current operating mode
ROB	reflection over the barrier
R1234yf	2,3,3,3-tetrafuoropropene
R1234ze(E)	trans-1,3,3,3-tetrafluoroprop-1-ene
R290	propane
TREC	thermally regenerative electrochemical cycle
TRER	thermally regenerative electrochemical refrigerator
TRERs	thermally regenerative electrochemical refrigerator with multiple cells

The remarkable performance of a thermodynamic system usually implies its promising reverse counterpart. Hence, it is natural to come up with the idea of reversing TREC for cooling purpose. Surprisingly, the literature review shows that compared to the tremendous theoretical and experimental research progress of TREC, the studies on its reversed system, i.e., thermally regenerative electrochemical refrigerator (TRER), are hardly developed. Insightful inspections reveal that the underlying reason for this little progress is the absence of a practically feasible TRER model serving as the cornerstone for further development. After scrutinizing the thermally regenerative electrochemical system, it turns out to be impossible to achieve independent refrigeration in practice by simply reversing TREC. Three major obstacles encountered are as follows: (1) the unavoidable regeneration losses; (2) heat cannot flow from a cold object to a hot one spontaneously; (3) the temperature of the thermogalvanic cell cannot be changed by compression and expansion, a feature well different from the gaseous working substance.

Attending the above comments, breaking through the bottleneck of the thermodynamic modeling and investigating the performance characteristics of TRER are of theoretical and practical significance. In the present work, a TRER model with practical feasibility is established for the first time by innovatively introducing the counterparts of traditional adiabatic compression and expansion processes in electrochemical systems, i.e., the adiabatic pre-charging and pre-discharging processes. Moreover, to achieve continuous refrigeration, the thermally regenerative electrochemical refrigerator model with multiple thermogalvanic cells (TRERs) is further constructed. Based on the proposed TRERs model, the cooling power, coefficient of performance (COP), and continuous refrigeration criterion are analytically derived. The main performance characteristics and optimally operating region are obtained and discussed. In addition, the COPs of various refrigeration systems reported in previous research are collected to highlight the competitive performance of the proposed TRERs. The present work not only lays the foundation for the experimental investigations and further developments of TRER but also paves the way for the construction of other novel thermally regenerative electrochemical cycle systems.

2. Materials and methods

2.1. Electrode materials

The thermogalvanic cell with highly reversible electrode materials proposed in Ref. [11] is employed to construct TRER in the present work. Specifically, copper hexacyanoferrate (CuHCF) and copper/cupric (Cu/Cu^{2+}), with the benefits of low heat capacity, high charge capacity, and high absolute value of temperature coefficient, are selected as the active materials of cathode and anode, respectively. Consequently, the values of internal resistance, temperature coefficient, specific heat capacity, and specific charge capacity of the thermogalvanic cell can be determined [11].

2.2. TRER(s) model construction and operation

The TRER model constructed by simply reversing TREC is schematically depicted in Fig. 1, where 1–2 and 3–4 are two isothermal processes with constant temperatures T_c and T_h, respectively; 2–3 and 4–1 are two regenerative processes; T_H and T_C are the temperatures of the hot and cold heat reservoirs, respectively. Nevertheless, after scrutinizing the details of the TRER shown in Fig. 1, it turns out to be practically infeasible to complete a refrigeration cycle due to the following reasons: 1. the regeneration loss is inevitable in practice; 2. heat cannot flow from a cold object to a hot one spontaneously. Consequently, considering the non-ideal regeneration and the facts $T_h > T_H$ and $T_c < T_C$, the objective temperatures of the cell (i.e., T_h and T_c) are not attainable without the support of auxiliary heating and cooling devices [31]. In other words, the four processes shown in Fig. 1 are not enough to form a proper and feasible TRER device. Additionally, different from the gaseous working substance, the temperature of the cell cannot be changed by compression and expansion, which makes trouble for the thermodynamic modeling of TRER.

In order to overcome the abovementioned flaws and bottlenecks, a novel TRER model is proposed in this work, as shown in Fig. 2a. Specifically, the thermogalvanic cell undergoes six processes to complete a refrigeration cycle. In process 1–2, the cell is charged at a constant temperature T_c while absorbing heat from the cooled space with temperature T_C resulting from the electrochemical reaction. After being charged, the cell is heated up from T_c to $T_h^{'}$ at open circuit condition in process 2–3 by means of the absorbed regeneration heat Q_{re}. To attain the objective temperature T_h, an additional process 3–4 named pre-discharging process is introduced, during which the cell is discharged adiabatically. Accordingly, the cell temperature is raised in this process by absorbing the Joule heat and electrochemical reaction heat. And then the cell is discharged at constant temperature T_h by delivering heat into the environment with temperature T_H in process 4–5. Process 5–6 is just opposite to process 2–3, so the cell temperature decreases from T_h to $T_c^{'}$ by releasing the regenerative heat. At the end, another additional process 6–1 is essential for the cell to go back to the initial state with temperature T_c. In such process, named as pre-charging process, the cell is charged adiabatically and cooled down from $T_c^{'}$ to T_c due to thermogalvanic effect. Additionally, Q_L in Fig. 2a stands for the external heat leakage between two reservoirs. The absorbed and released heat in the abovementioned six processes will be given in detail in the next subsection. Moreover, it is worth mentioning that the rise and fall of the cell temperature in the pre-charging and pre-discharging processes can be partly replaced by adding another two heat exchanging processes between the cell and two heat reservoirs. Whereas, the complexities of the system will be greatly enhanced by constructing such an eight-process TRER model.

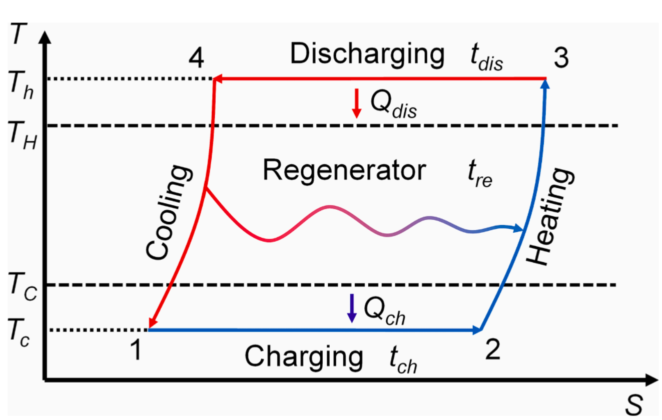

Fig. 1. The T-S diagram of a four-process TRER constructed by simply reversing TREC.

It is interesting to point out that the proposed adiabatic pre-charging and pre-discharging processes can be regarded as the counterparts of traditional adiabatic compression and expansion processes since the temperatures of working substances are all changed by the input or output work in these processes. However, the temperature variations of the cell due to the input and output work are just opposite to the traditional adiabatic compression and expansion processes because of the negative temperature coefficient in the present case.

Owning to the negative temperature coefficient, the voltages of the charging and pre-charging processes are higher than the corresponding voltages of the discharging and pre-discharging processes. As a consequence, the TRER is driven by external power to fulfill refrigeration after going through the aforementioned six processes.

Nevertheless, the reciprocating operation of the abovementioned TRER cycle implies intermittent refrigeration. Moreover, the thermal energy storage device is necessary for the regeneration. Regarding this issue, a TRER system with continuous refrigeration is further established by employing more cells, which is denoted by TRERs and shown in Fig. 2b. Specifically, N identical thermogalvanic cells divided into identical N/M cell packs are used to construct the TRERs model. The M thermogalvanic cells packed together experience the charging, discharging, pre-charging, and pre-discharging processes simultaneously. Note in Fig. 2b that there are always M thermogalvanic cells contacting and absorbing heat from the cooled space during an overall cycle. Accordingly, continuous refrigeration can be achieved.

2.3. Main performance parameters and continuous refrigeration condition

In this subsection, the analytical expressions of cooling power and COP are derived based on the established TRERs model.

By considering thermogalvanic and Joule heat effects, the net heat released into the environment and absorbed from cooled space by one cell pack in a cycle are given by [20,21,25]

$$Q_{dis} = M(|\alpha_c|T_h I_{dis} t_{dis} + I_{dis}^2 R_{int} t_{dis}) \tag{1}$$

and

$$Q_{ch} = M(|\alpha_c|T_c I_{ch} t_{ch} - I_{ch}^2 R_{int} t_{ch}) \tag{2}$$

respectively, where t_{ch} and t_{dis} are the time durations of charging and discharging processes for one cell pack, respectively, I_{ch} and I_{dis} denote the corresponding currents, and R_{int} indicates the internal resistance of one cell. Additionally, in Eqs. (1) and (2), α_c is the temperature coefficient, which is assumed to be a constant and can be expressed as [11,25]

$$\alpha_c = \frac{\partial V_{oc}}{\partial T} = \frac{\sum v_j s_j}{n_e F} \tag{3}$$

where V_{oc} is the open circuit voltage of one cell, n_e denotes the number of electrons transferred in the reaction, F stands for Faraday constant, v_j and s_j are the stoichiometric number and partial molar entropy of the jth chemical involved.

Moreover, the heat transferred between the cell pack and two heat sources are assumed to obey linear heat transfer law, namely,

$$Q_{dis} = MK_h(T_h - T_H)t_{dis} \tag{4}$$

and

$$Q_{ch} = MK_c(T_C - T_c)t_{ch} \tag{5}$$

where K_h and K_c are the associated heat transfer coefficients. The cell temperatures in the charging and discharging processes can be deduced based on Eqs. (1), (2), (4), and (5), namely,

$$T_h = \frac{K_h T_H + I_{dis}^2 R_{int}}{K_h - |\alpha_c| I_{dis}} \tag{6}$$

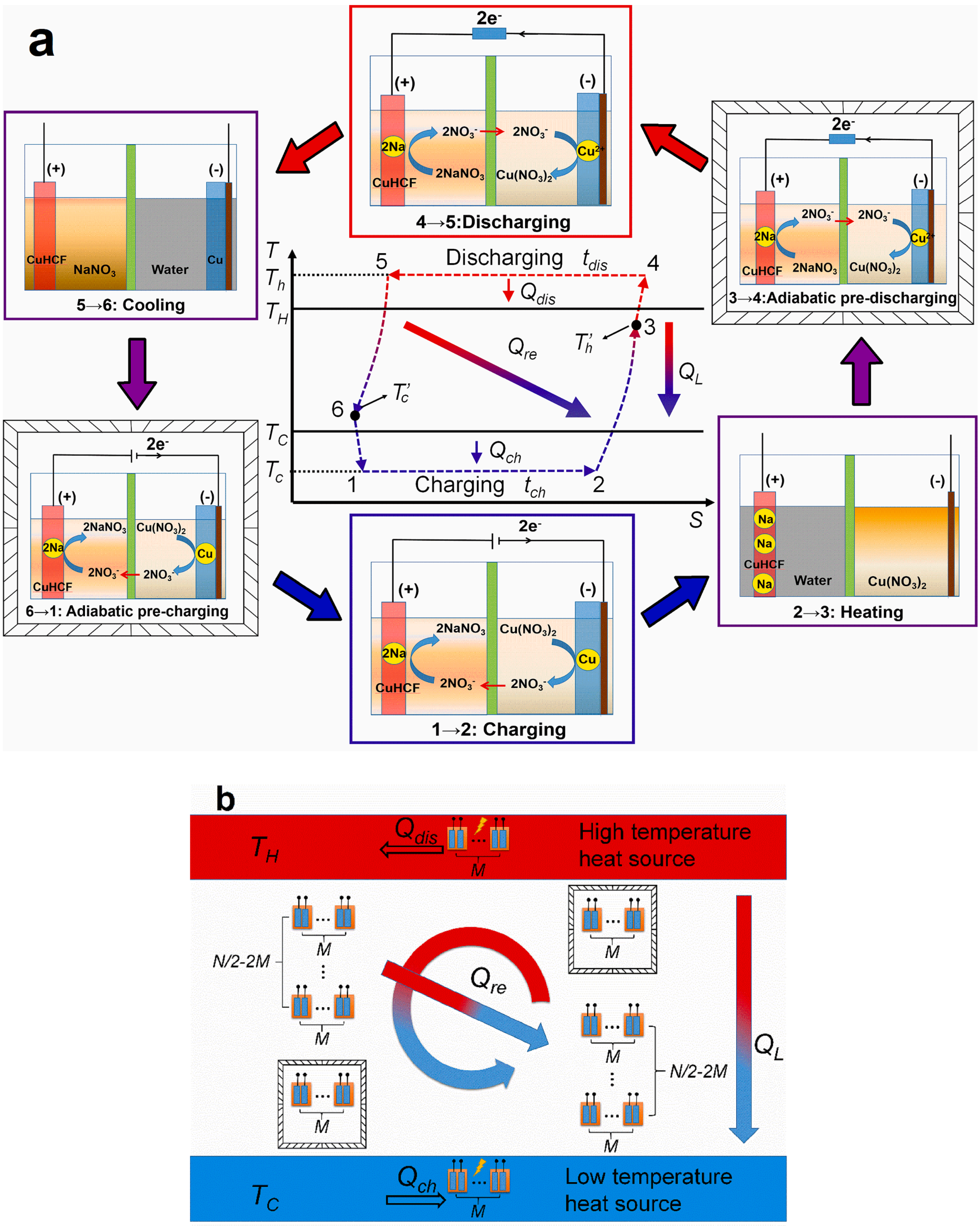

Fig. 2. (a) The T-S and schematic diagrams of the proposed six-process TRER and (b) the schematic diagram of a continuous refrigeration TRER with N thermo-galvanic cells (TRERs), where Q_{re} and Q_L denote the regeneration heat and the external heat leakage in one cycle.

and

$$T_c = \frac{K_c T_C + I_{ch}^2 R_{int}}{K_c + |\alpha_c| I_{ch}} \quad (7)$$

respectively.

As shown in Fig. 2, the charging (discharging) process is followed by the regenerative heating (cooling) process. Nevertheless, ideal regeneration can be only achieved with infinite regenerative time and infinite cell packs, which implies practical infeasibility. Accordingly, the non-ideal regeneration should be considered, and the corresponding regenerative efficiency is defined as [20,21]

$$\eta_{re} = \frac{2t_{re}}{\tau} \quad (8)$$

where t_{re} and τ are the regenerative time and overall cycle time, respectively.

Due to non-ideal regeneration, the temperatures of the cell packs after regeneration are

$$T_h' = T_c + (T_h - T_c)\eta_{re} \quad (9)$$

and

$$T_c' = T_h - (T_h - T_c)\eta_{re} \quad (10)$$

respectively. To reach the objective temperatures T_h and T_c, the additional thermal energy

$$Q_{ad} = MC_p(1 - \eta_{re})(T_h - T_c) \quad (11)$$

is required to be absorbed and released by the cell pack, respectively. In Eq. (11), C_p is the heat capacity of one cell. Note in Eq. (11) that $Q_{ad} = 0$ when $\eta_{re} = 1$. Nevertheless, this part of thermal energy cannot be compensated by the heat exchanging processes with two heat reservoirs due to $T_h > T_H$ and $T_c < T_C$. Moreover, the traditional approach for the gaseous working substance by compression and expansion is not suitable in the present case. Consequently, the effects of heating by discharging and cooling by charging are the key notion for the construction of the TRER(s). Specifically, the adiabatic pre-charging and pre-discharging processes are innovatively introduced to lower and raise the temperature of the cell, respectively.

At reversible condition, the dependence of the temperature variation on the amount of charge transferred can be deduced by using the adiabatic condition, isobaric condition, and Maxwell relation, namely

$$dT = \left(\frac{\partial S}{\partial T}\right)_{Q_e}^{-1}\left(\frac{\partial V}{\partial T}\right)_{Q_e} dQ_e = \frac{T}{C_p}\alpha_c dQ_e \quad (12)$$

where Q_e is the electrode charge, dQ_e is the amount of charge transferred from negative electrode to positive electrode, S and V are the entropy and voltage of one cell, respectively. In order to take the irreversibility into account while rendering more feasible calculations, the average temperatures $(T_c + T_c')/2$ and $(T_h + T_h')/2$ are adopted, respectively, to calculate the net thermal energies consumed and generated by one cell pack during the pre-charging and pre-discharging processes approximatively, i.e.,

$$Q_{pch} = \frac{1}{2}M|\alpha_c| I_{pch} t_{pch}(T_c + T_c') - MI_{pch}^2 R_{int} t_{pch} \quad (13)$$

and

$$Q_{pdis} = \frac{1}{2}M|\alpha_c| I_{pdis} t_{pdis}(T_h + T_h') + MI_{pdis}^2 R_{int} t_{pdis} \quad (14)$$

where t_{pch} and t_{pdis} are the time durations of the pre-charging and pre-discharging processes for one cell pack; and I_{pch} and I_{pdis} denote the corresponding currents. In Eqs. (13) and (14), the first terms are the thermal energies consumed and generated due to thermogalvanic effect, while the second terms correspond to the associated Joule heat.

By considering the adiabatic condition, the generated and consumed thermal energies lead to the rise and fall of the cell temperature, respectively. To reach the objective temperatures T_h and T_c, the relation

$$Q_{pch} = Q_{pdis} = Q_{ad} \quad (15)$$

should be satisfied.

Additionally, steady and continuous operation requires that $t_{ch} = t_{dis} = t_{pch} = t_{pdis} \equiv t$. Besides, noting that all the cell packs inside the TRERs are equivalent and there are M cells experiencing the charging, discharging, pre-charging, and pre-discharging processes simultaneously, one has

$$t = \frac{M}{N}\tau \quad (16)$$

and

$$\tau = 4t + 2t_{re} \quad (17)$$

The substitution of Eqs. (16) and (17) into Eq. (8) yields

$$\eta_{re} = 1 - \frac{4M}{N} \quad (18)$$

It can be realized from Eq. (18) that the regenerative efficiency approaches 1 at the condition $M/N \rightarrow 0$, as expected. In contrast, Eq. (18) also indicates that the minimum value of N/M is 4 with corresponding regenerative efficiency $\eta_{re} = 0$. In this case, the six-process cycle degenerates into a four-process cycle. In addition, the following relation

$$N - 4M = 2kM \ (k = 0, 1, 2 \ldots) \quad (19)$$

can be deduced by considering the continuous refrigeration operation and the regenerative symmetry of the system. In Eq. (19), $2kM$ denotes the cells going through the regenerative processes, while $4M$ represents the 4 cell packs experiencing the charging, discharging, pre-charging, and pre-discharging processes simultaneously.

Besides, it is necessary to further consider the external heat leakage loss between the environment and the cooled space existing inevitably in practice. By assuming Newton's law, the external heal leakage in one cycle can be expressed as

$$Q_L = K_L(T_H - T_C)\tau \quad (20)$$

where K_L is the associated heat leakage coefficient.

Based on the above discussions, three important performance indicators, namely, the cooling power, power input, and COP of the TRERs, can be obtained as

$$R = \frac{Q_{ch}}{t} - \frac{Q_L}{\tau} = M(|\alpha_c| T_c I_{ch} - I_{ch}^2 R_{int}) - K_L(T_H - T_C) \quad (21)$$

$$P = \frac{Q_{dis} - Q_{ch}}{t} = M[|\alpha_c|(T_h I_{dis} - T_c I_{ch}) + (I_{dis}^2 + I_{ch}^2)R_{int}] \quad (22)$$

and

$$\varepsilon = \frac{R}{P} = \frac{M(|\alpha_c| T_c I_{ch} - I_{ch}^2 R_{int}) - K_L(T_H - T_C)}{M[|\alpha_c|(T_h I_{dis} - T_c I_{ch}) + (I_{dis}^2 + I_{ch}^2)R_{int}]} \quad (23)$$

respectively.

3. Results and discussion

3.1. Constraints between four currents

Note in Eqs. (6), (7), and (21)–(23) that I_{ch} and I_{dis} are two control parameters for a given TRERs. Whereas, I_{ch} and I_{dis} are constrained by the law of charge conservation, i.e.,

$$C_q/t = I_{ch} + I_{pch} = I_{dis} + I_{pdis} \quad (24)$$

where C_q is the charge capacity of one cell.

Substituting Eqs. (9)-(11), (13), (14), (16), and (24) into Eq. (15), one has

$$(1-\eta_{re})\frac{c_p}{c_q}(T_h - T_c)(I_{dis} + I_{pdis}) = \frac{1}{2}|\alpha_c|I_{pdis}[T_h + T_c + (T_h - T_c)\eta_{re}] + I_{pdis}^2 R_{int} \quad (25)$$

and

$$(1-\eta_{re})\frac{c_p}{c_q}(T_h - T_c)(I_{ch} + I_{pch}) = \frac{1}{2}|\alpha_c|I_{pch}[T_h + T_c - (T_h - T_c)\eta_{re}] - I_{pch}^2 R_{int} \quad (26)$$

where c_p and c_q are the specific heat and charge capacity of the cell, respectively. Notably, Eqs. (24)-(26) imply only one independent current for a given TRERs. More specifically, all parameters of the system will be determined if only one of the four currents is given.

In the following discussions, I_{ch} is selected as the control parameter since Eqs. (7) and (21) indicate that the cooling power can be uniquely determined by I_{ch} for a given TRERs. Unfortunately, the analytical solutions of I_{pch}, I_{dis}, and I_{pdis} as the functions of I_{ch} are not analytically available. In consequence, numerical calculation is used to analyze the performance characteristics of the TRERs.

By using Eqs. (6), (7), (18), (24)-(26), and conservation of charge, the dependences of I_{pch}, I_{dis}, and I_{pdis} on I_{ch} are numerically generated, as shown in Fig. 3. It can be seen from Fig. 3 that there exists a maximum value of charging current $I_{ch,\max}$ corresponding to the unique solutions of I_{pch}, I_{dis}, and I_{pdis}. Nevertheless, for other values of $I_{ch} < I_{ch,\max}$ there are two possible solutions of I_{pch}, I_{dis}, and I_{pdis} corresponding to high-current (HC) and low-current (LC) operating modes, respectively. Moreover, when $I_{ch} > I_{ch,\max}$ the physically acceptable solutions of I_{pch}, I_{dis}, and I_{pdis} cannot be found, which implies the TRERs is disabled.

3.2. $R - I_{ch} - \eta_{re}$ performance characteristics

The behaviors of R varying with I_{ch} and η_{re} are presented in Fig. 4 by using Eqs. (6), (7), (18), (21), (24)-(26). It is shown by Fig. 4 that for a given value of K_L, R is fully determined by I_{ch} and independent of η_{re}. This behavior is consistent with Eqs. (7) and (21). Nevertheless, the value of $I_{ch,\max}$ increases as η_{re} grows, which can be explained as follows. With the decrease of η_{re}, more capacity of the cell needs to be distributed to the pre-charging and pre-discharging processes to achieve the objective temperatures. In consequence, the value of I_{ch} is limited in the light of Eqs. (24) and (26).

Moreover, Fig. 4a indicates that when the value of $I_{ch,\max}$ (η_{re}) is small, R is a monotonically increasing function of I_{ch}. In this case, $I_{ch,\max}$ is just the charging current making R maximum, namely $I_{ch,\max} = I_{ch,Rm}$. Note that with the increase of $I_{ch,\max}$ (η_{re}), the curves of $R - I_{ch}$ become gradually parabolic-like, as expected. The parabolic-like behaviors result from the competition between thermogalvanic and Joule heat effects shown by Eq. (21). Besides, the parabolic-like curves of $R - I_{ch}$ imply the optimal charging current $I_{ch,Rm}$ at which R attains its maximum value. Note that $I_{ch,\max}$ is different from $I_{ch,Rm}$ in this situation. In addition, it can be realized from Fig. 4b that for the parabolic-like curves of $R - I_{ch}$, $R_{\max}$ and the corresponding $I_{ch,Rm}$ are practically independent on η_{re}.

3.3. $R - I_{ch} - \varepsilon$ performance characteristics

With regard to the influence of I_{ch} on ε, the three-dimensional graphs of R varying with I_{ch} and ε are plotted based on Eqs. (6), (7), (18), (21), (23)-(26), which are shown by Fig. 5. It can be clearly seen from Fig. 5 that the variations of R with I_{ch} and ε depend on both the values of K_L and η_{re}. For the convenience of discussion, the three-dimension curves of R varying with I_{ch} and ε with different values of K_L and η_{re} are projected onto the $R - \varepsilon$ plane, which are depicted in Fig. 6.

Inspection of Figs. 5 and 6 shows that when the value of η_{re} is small ($\eta_{re} = 0.8$), the behaviors of R varying with ε are parabolic ($K_L = 0$) and loop-shaped ($K_L > 0$), respectively. Whereas the corresponding

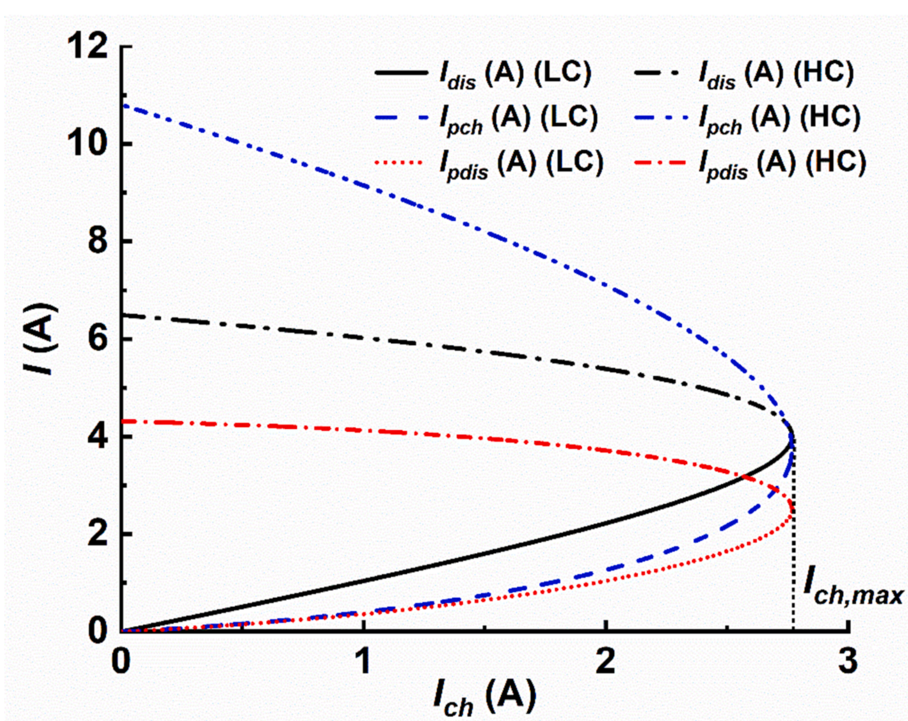

Fig. 3. Variations of I_{dis}, I_{pch} and I_{pdis} with I_{ch}, where HC and LC denote high-current and low-current modes, respectively. The values of parameters: $T_H = 303.15K$, $T_C = 283.15K$, $|\alpha_c| = 0.0012V/K$, $R_{int} = 0.015\Omega$, $c_p = 2048J/(K\cdot kg)$, $K_h = K_c = 0.1W/K$, $c_q = 116748C/kg$, $\eta_{re} = 0.8$ ($M = 1,\ N = 20$).

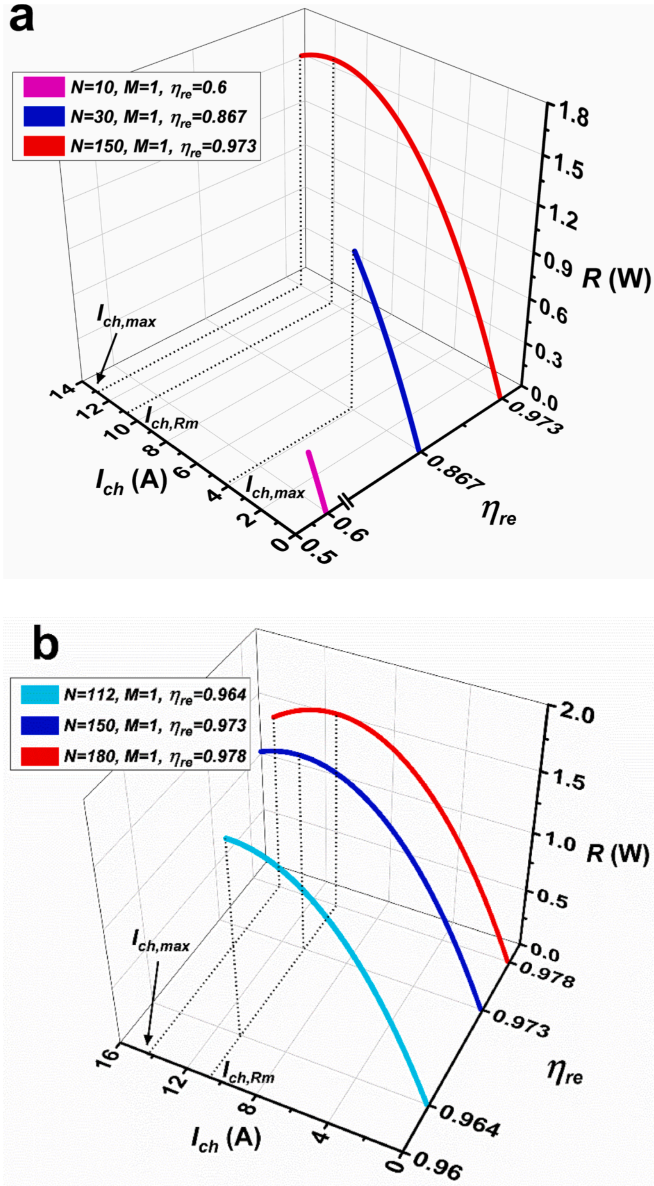

Fig. 4. 3-D plots of R varying with I_{ch} and η_{re}, where $K_L = 0.002W/K$. The other parameters have the same values as those adopted in Fig. 3.

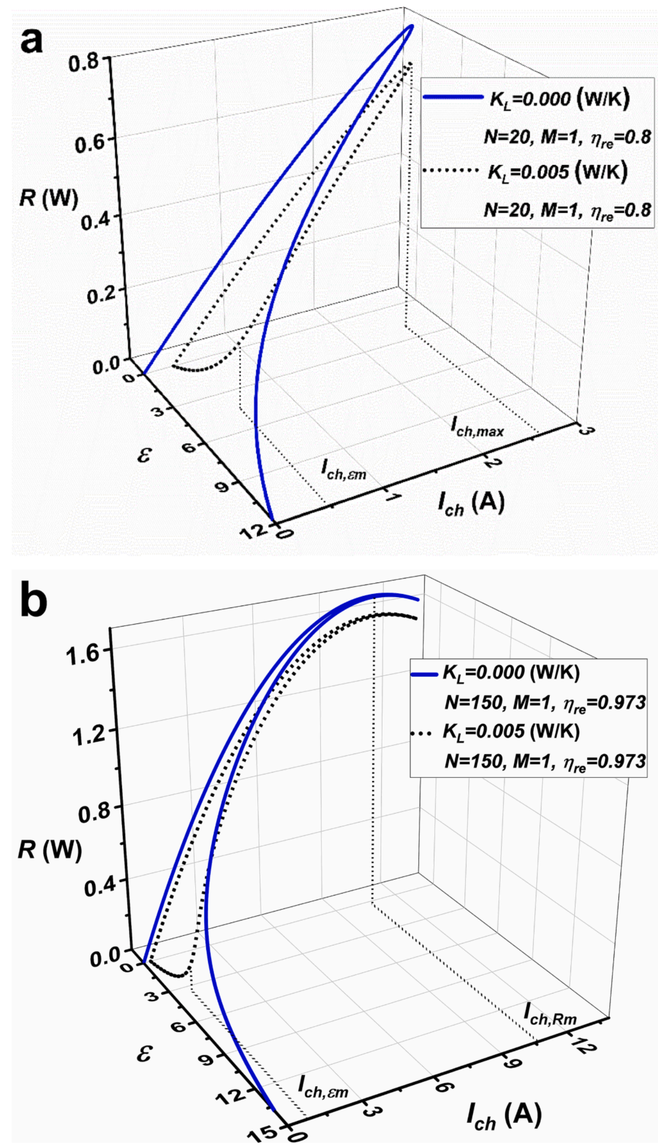

Fig. 5. 3-D plots of R varying with I_{ch} and ε for different values of K_L and η_{re}. The other parameters have the same values as those adopted in Fig. 3.

variations become more complicated with high enough regenerative efficiency ($\eta_{re} = 0.973$), which is shown by Figs. 5b and 6c, d. Despite the various behaviors, all the graphs in Fig. 5 indicate that there are two corresponding values of ε for a given value of I_{ch}. These two ε values just correspond to the high-current mode and low-current mode mentioned in Fig. 3. To explicitly illustrate the difference, the two operating modes are presented by different line styles in Fig. 6. Figs. 5 and 6 indicate that for a given value of I_{ch}, the system operating in the low-current mode possesses the same value of R but a higher value of ε regardless of the values of K_L and η_{re}. Accordingly, the TRERs should be always operated in the low-current mode. Hence, the following discussions will focus on the low-current mode.

On the basis of the above analyses, the optimally operating region of the TRERs at four different cases can be further determined from Figs. 5 and 6, respectively. Specifically, the solid $R-\varepsilon$ curve in Fig. 6a denotes that there exist an optimal COP ε_{Rm} leading to the maximum cooling power $R_{\max}$ and a maximum COP $\varepsilon_{\max}$ with zero cooling power. Notably, the optimally operating region of the TRERs system in this case can be determined, namely $\varepsilon_{Rm} < \varepsilon < \varepsilon_{\max}$ and $0 < R < R_{\max}$, which is literally the operating region of low-current mode. In this region, the point with the same value of cooling power but a higher value of COP can be found compared to the corresponding point outside. In addition, the associated operating values of I_{ch} can be further deduced from Figs. 5 and 6, i.e., $0 < I_{ch} < I_{ch,\max}$.

Similar discussions about the solid $R-\varepsilon$ curves in Fig. 6b–d can give rise to the optimally operating regions and the corresponding I_{ch} for the other three cases, which are directly listed as follows for saving the length. $\varepsilon_{Rm} < \varepsilon < \varepsilon_{\max}$ and $R_{\varepsilon m} < R < R_{\max}$ is the optimally operating region for Fig. 6b, c, while $\varepsilon_{Rm} < \varepsilon < \varepsilon_{\max}$ and $0 < R < R_{\max}$ is the one for Fig. 6d. The associated optimal values for the charging current are $I_{ch,\varepsilon m} < I_{ch} < I_{ch,\max}$ ($I_{ch,\max} = I_{ch,Rm}$ in this case) for Fig. 6b, $I_{ch,\varepsilon m} < I_{ch} < I_{ch,Rm}$ for Fig. 6c, and $0 < I_{ch} < I_{ch,Rm}$ for Fig. 6d.

3.4. Influence of parameter M

The above discussions concentrate on the situation with $M = 1$. Whereas the derivations and the expressions of performance indicators indicate that the number of cells inside one cell pack has great impact on the performance of the TRERs. Using the similar approach to Fig. 6, one can obtain the behaviors of R varying with ε for the different values of M,

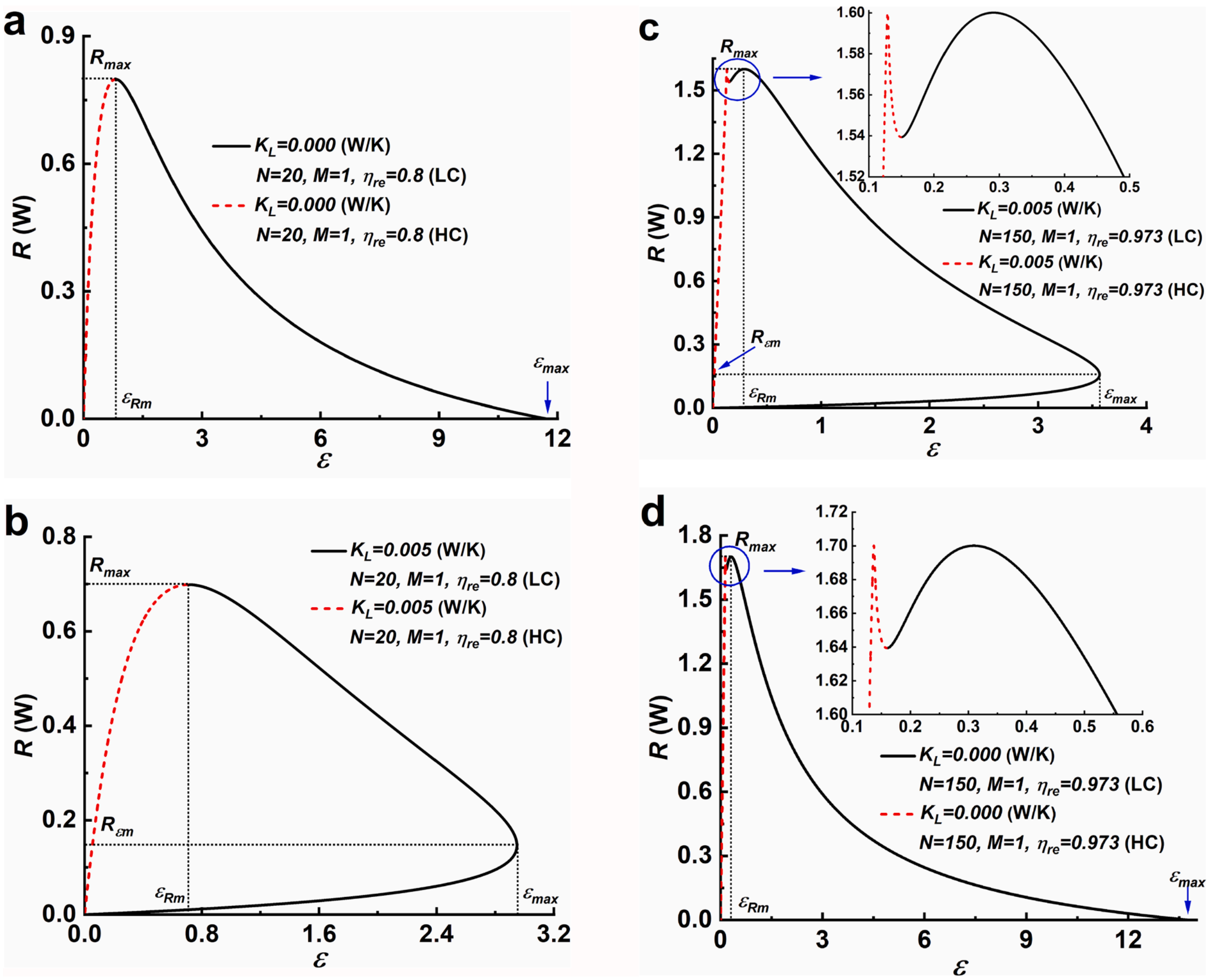

Fig. 6. The behaviors of R varying with ε for different values of K_L and η_{re}, where HC and LC denote high-current and low-current operating modes, respectively. The other parameters have the same values as those adopted in Fig. 3.

which is shown by Fig. 7. It can be realized from Fig. 7 that for the same value of η_{re} (i.e., the same value of M/N), $R_{\max}$, $\varepsilon_{\max}$, $R_{\varepsilon m}$, and ε_{Rm} all increase with M. In other words, the performance of the TRERs can be further enhanced by employing more cells for a given value of η_{re} (i.e., a given value of M/N). Notably, this result is consistent with Eqs. (21) and (23) but may slightly deviate from the practical case since K_L is assumed to be a constant and independent of the size of the system (the value of N) for the convenience of discussion in the present study.

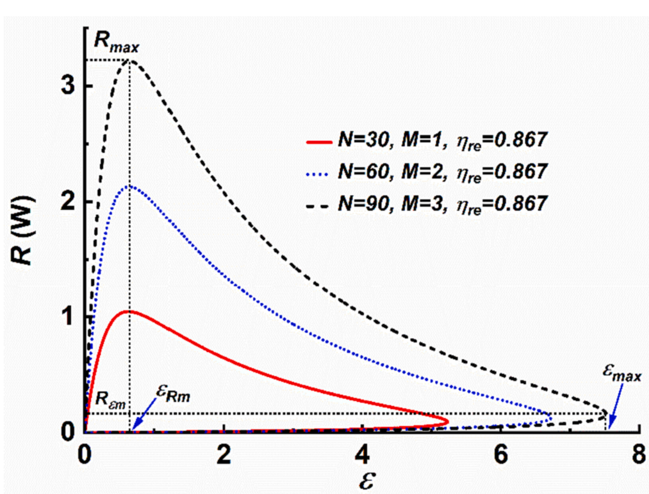

Fig. 7. The behaviors of R varying with ε for different values of N and M, where $K_L = 0.002W/K$. The other parameters have the same values as those adopted in Fig. 3.

3.5. Influence of η_{re} on $R_{\max}$, $\varepsilon_{\max}$, $R_{\varepsilon m}$, and ε_{Rm}

On the basis of the above analyses, the variations of $R_{\max}$, $\varepsilon_{\max}$, $R_{\varepsilon m}$, and ε_{Rm} with η_{re} can be further generated by using Eqs. (6), (7), (18), (21), (23)-(26). This is shown in Fig. 8. Note that not all the values of η_{re} are feasible due to the limitation of Eq. (19). Besides, it can be seen from Fig. 8a,b that the behaviors of $R_{\max}$ and ε_{Rm} varying with η_{re} are quite different in the regions of $\eta_{re} < 0.964$ and $\eta_{re} > 0.964$. Specifically, when $\eta_{re} < 0.964$, the allowed maximum charging current $I_{ch,\max}$ ($I_{ch,\max} = I_{ch,Rm}$ in this case) grows with the increasing of η_{re} (see Fig. 4), which leads to the prominent rise of $R_{\max}$. Whereas, the growing of $I_{ch,\max}$ also gives rise to a higher Joule heat effect. The parabolic variation of ε_{Rm} with η_{re} results from the competition between the regenerative efficiency and Joule heat effect. On the other hand, when $\eta_{re} > 0.964$, the associated charging current for maximum cooling power is no longer $I_{ch,\max}$ but $I_{ch,Rm}$ ($I_{ch,\max} \neq I_{ch,Rm}$ in this case) whose variation with η_{re} is negligible (Fig. 4b). Hence, the variation of $R_{\max}$ with η_{re} becomes imperceptible and ε_{Rm} increases with η_{re} due to the reduction of irreversibility. Besides, Fig. 8c shows that both $\varepsilon_{\max}$ and $R_{\varepsilon m}$ increase with the increasing of η_{re}.

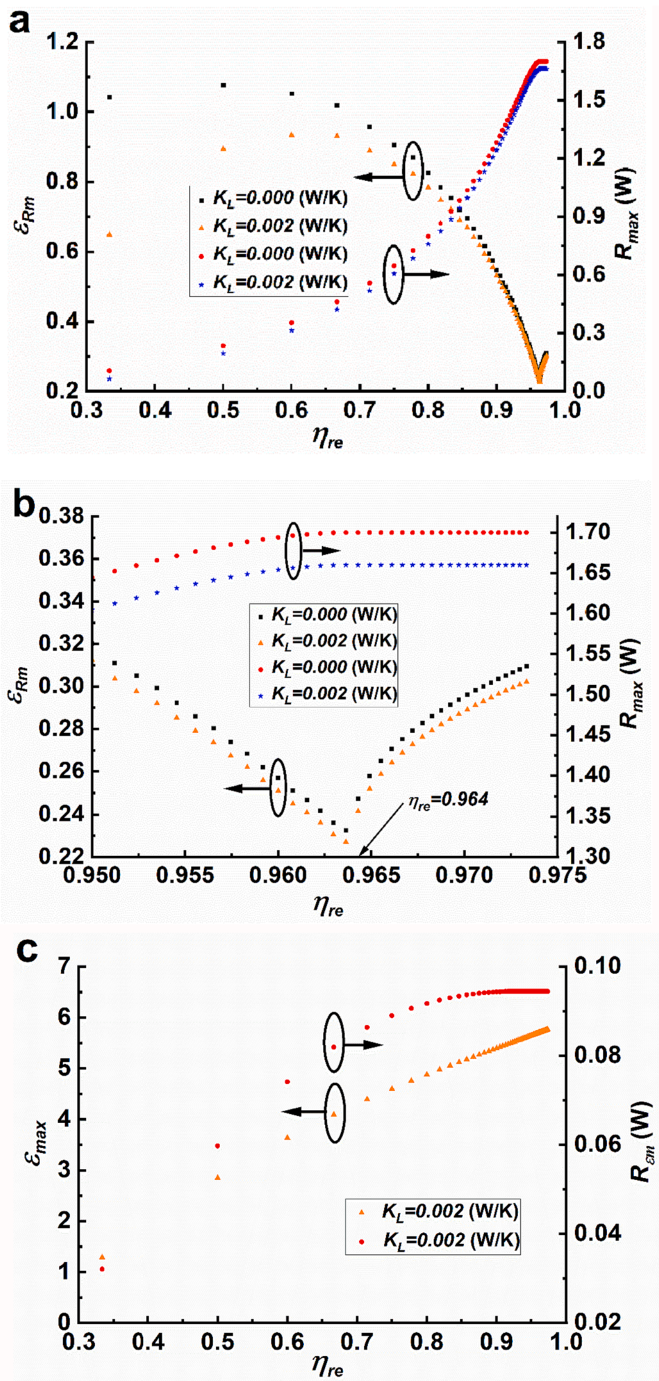

Fig. 8. The variations of (a and b) $R_{\max}$ and ε_{Rm} with η_{re} and (c) $\varepsilon_{\max}$ and $R_{\varepsilon m}$ with η_{re}, where $M = 1$. The other parameters have the same values as those adopted in Fig. 3.

3.6. Comparison with various refrigeration systems

To highlight the performance of the proposed TRERs more visible, the variations of $\varepsilon_{\max}/\varepsilon_{Car}$ and $\varepsilon_{Rm}/\varepsilon_{Car}$ with ε_{Car} are further presented in Fig. 9, where $\varepsilon_{Car} = T_C/(T_H - T_C)$ stands for the corresponding Carnot COP for the given temperatures. It can be seen from Fig. 9 that $\varepsilon_{\max}/\varepsilon_{Car}$ decreases with the decline of ε_{Car} while $\varepsilon_{Rm}/\varepsilon_{Car}$ grows with it. According to the discussions on Fig. 6, one can realize that the shadow area corresponds to the optimal region of the TRERs. In particular, Fig. 9 indicates that ε_{Rm} can exceed 5% of the Carnot COP, while $\varepsilon_{\max}$ can achieve up to 40% of the Carnot COP for the given values of parameters.

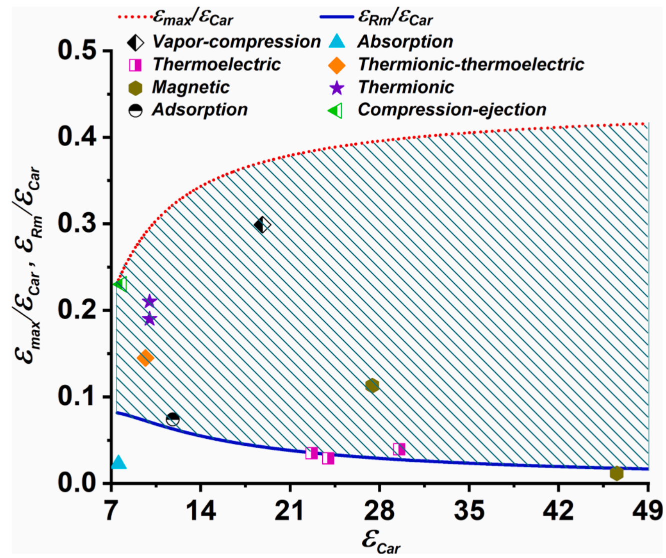

Fig. 9. The variations of $\varepsilon_{\max}/\varepsilon_{Car}$ and $\varepsilon_{Rm}/\varepsilon_{Car}$ with ε_{Car} and the reported COPs listed in Table 1, where $K_L = 0.002W/K$ and $\eta_{re} = 0.8$ ($M = 1,\ N = 20$). The other parameters have the same values as those adopted in Fig. 3.

Moreover, several COPs of various refrigeration systems reported in previous experimental and simulated research are collected to highlight the attractive performance of the TRERs, which are listed in Table 1 and marked by the various symbols in Fig. 9. Notably, the comparisons in Fig. 9 further illustrate the great potential of the proposed TRERs for efficient refrigeration.

3.7. Influence of electrode materials

Additionally, to discuss the influence of electrode materials on the performance of the TRERs, the behaviors of R varying with ε for the different values of α_c, R_{int}, c_p, and c_q are generated by using Eqs. (6), (7), (18), (21), (23)-(26), as shown in Fig. 10 a–d. It can be realized from Fig. 10 a–d that the performance of the TRERs can be improved by increasing the values of $|\alpha_c|$ and c_q or by decreasing the values of R_{int} and c_p. Consequently, it is of great significance for the performance improvement of the TRER(s) system to explore material with larger $|\alpha_c|$ and c_q and lower R_{int} and c_p. This result is similar to the conclusions in terms of TREC systems [42,43].

4. Conclusions

In summary, a novel strategy to overcome the three fundamental obstacles in constructing TRER model is proposed. Accordingly, the reciprocating TRER model followed by the TRERs model with continuous refrigeration were presented for the first time. Based on the proposed TRERs model, the expressions of the main performance indicators are analytically derived. In addition, two operating models (LC and HC) and four distinct behaviors of cooling power varying with COP of the TRERs (Fig. 6a–d) are indicated by numerical analyses. On this basis, the optimal operating model and optimal operating region along with the associated values of charging current were discussed and determined. Significantly, the COP at maximum cooling power and the maximum COP are predicted to achieve up to 5% and 40% of Carnot COP for the given values of parameters. Moreover, the comparison between the predicted results and the reported COPs of various refrigeration systems reveal the great potential of the TRERs for efficient refrigeration. Our work will hopefully serve as the cornerstone for further theoretical and experimental investigations and open a new avenue for the construction of other novel electrochemical cycles.

Table 1
Reported COPs of various refrigerators and the ratio to corresponding Carnot COPs.

Type of refrigerator	refrigerant	Type of analysis	Reported COP (ε_{rep})	Corresponding Carnot COP ε_{Car}	$\varepsilon_{rep}/\varepsilon_{Car}$
Vapor compression refrigerator [32]	R1234yf	Simulated	5.63	18.83	0.299
Absorption refrigerator [33]	R1234ze(E)	Simulated	0.17*	7.557**	0.0225
Adsorption refrigerator [34]	Water	Simulated	0.8715	11.81**	0.0738
Compression-ejection hybrid refrigerator [35]	R290	Simulated	1.8*	7.826	0.23
Thermoelectric refrigerator [36]	N/A	Simulated	0.69	23.98	0.0288
Thermoelectric refrigerator [37]	CP2-127 Peltier modules	Experimental	0.79	22.69	0.0348
Thermoelectric refrigerator [37]	CP2-127 Peltier modules	Experimental	1.16	29.53	0.0393
Thermionic-thermoelectric refrigerator [38]	Ideal materials	Simulated	1.4*	9.667	0.145
Thermionic refrigerator [39]	Single barrier structure with ROB	Simulated	1.9*	10.00	0.190
Thermionic refrigerator [39]	Single barrier structure without ROB	Simulated	2.1*	10.00	0.210
Magnetic regenerator [40]	Gd, Gd-based alloys, and their composites	Experimental	3.1	27.43	0.113
Magnetic regenerator [41]	Gd	Experimental	0.54	46.55	0.0116

* Data read from the figures in associated references approximately.
** The Carnot COPs are calculated by using the temperatures of working fluid due to the lack of the temperatures of heat reservoirs.

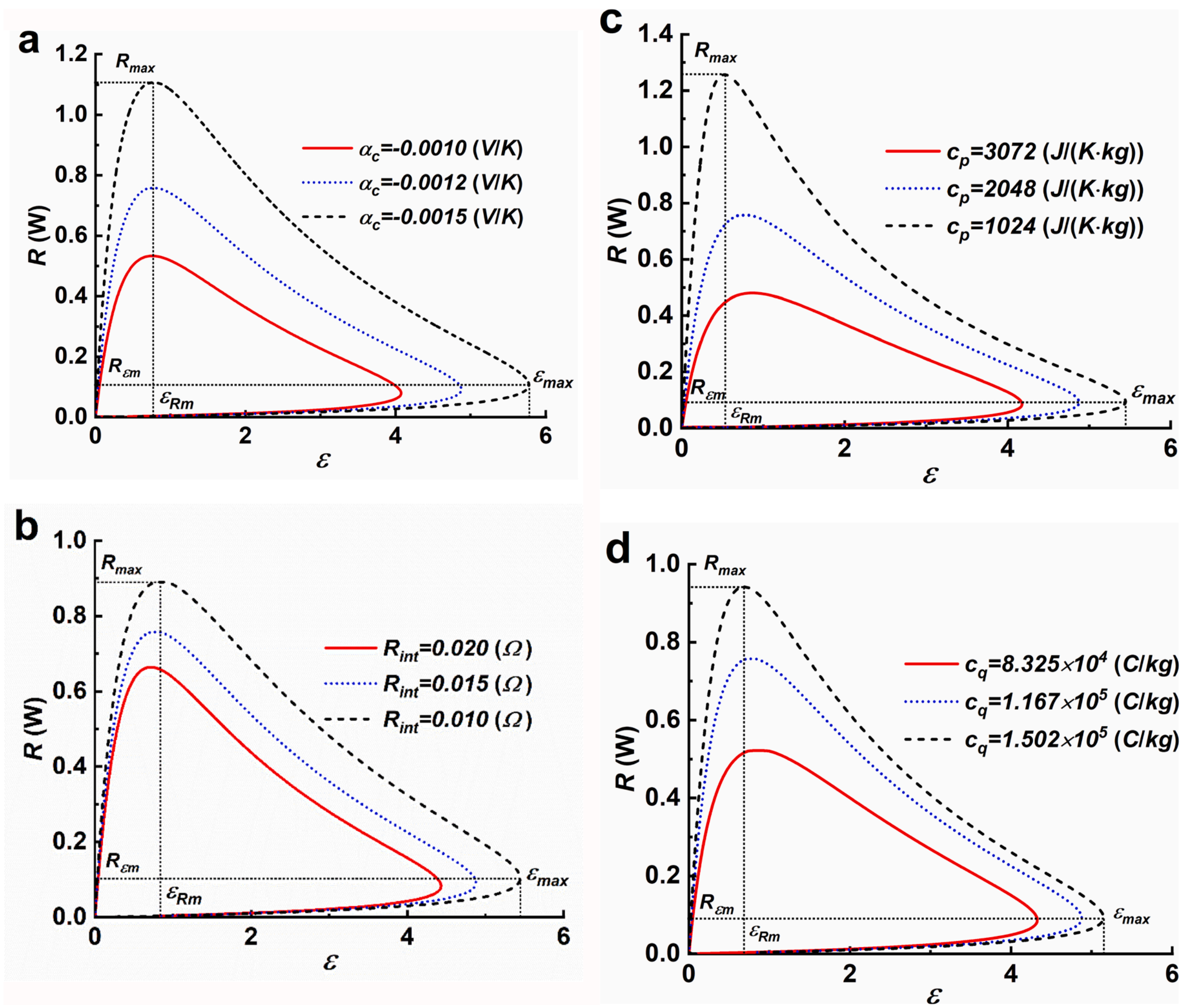

Fig. 10. The behaviors of R varying with ε for different values of (a) $|\alpha_c|$, (b) R_{int}, (c) c_p, and (d) c_q, where $K_L = 0.002W/K$. The other parameters have the same values as those adopted in Fig. 3.

CRediT authorship contribution statement

Bo Chen: Methodology, Software, Validation, Formal analysis, Investigation, Writing – original draft. **Julian Gonzalez-Ayala:** Methodology, Validation, Writing – review & editing. **A. Calvo Hernández:** Methodology, Validation, Writing – review & editing. **Rongxiang Luo:** Software, Validation, Writing – review & editing. **Hanxin Yang:** Software, Validation, Writing – review & editing. **Juncheng Guo:** Conceptualization, Methodology, Validation, Formal analysis, Writing – review & editing, Supervision, Project administration, Funding acquisition.

Declaration of Competing Interest

The authors declare that they have no known competing financial interests or personal relationships that could have appeared to influence the work reported in this paper.

Data availability

Data will be made available on request.

Acknowledgements

This work has been supported by the Natural Science Foundation of Fujian Province (Grant No. 2022J01547) and the National Natural Science Foundation of China (Grant No. 61773121). JGA thanks financial support from NEXTGENERATION EU funds under project MIA.2021. M01.0004.E24.

References

[1] Birol F. The future of cooling: opportunities for energy-efficient air conditioning. International Energy Agency; 2018. https://doi.org/10.1787/9789264301993-en.
[2] Polvani LM, Previdi M, England MR, Chiodo G, Smith KL. Substantial twentieth-century Arctic warming caused by ozone-depleting substances. Nat Clim Change 2020;10:130–3.
[3] Goyal P, Baredar P, Mittal A, Siddiqui AR. Adsorption refrigeration technology – an overview of theory and its solar energy applications. Renew Sust Energ Rev 2016;53:1389–410.
[4] Bell LE. Cooling, heating, generating power, and recovering waste heat with thermoelectric systems. Science 2008;321:1457–61.
[5] Chen L, Lorenzini G. Comparative performance for thermoelectric refrigerators with radiative and Newtonian heat transfer laws. Case Stud Therm Eng 2022;34:102069.
[6] Gómez JR, Garcia RF, Catoira DM, Gómez MR. Magnetocaloric effect: a review of the thermodynamic cycles in magnetic refrigeration. Renew Sust Energ Rev 2013;17:74–82.
[7] Lin J, Tong P, Zhang K, Tao K, Lu W, Wang X, et al. Colossal and reversible barocaloric effect in liquid-solid-transition materials n-alkane. Nat Commun 2022;13:596.
[8] Qi C, Chen L, Ge Y, Huang L, Feng H. Thermal Brownian refrigerator with external and internal irreversibilities. Case Stud Therm Eng 2022;36:102185.
[9] Qiu S, Ding Z, Chen L, Ge Y. Performance optimization of thermionic refrigerators based on van der Waals heterostructures. Sci China-Technol Sci 2021;64:1007–16.
[10] Qiu S, Ding Z, Chen L, Meng F, Sun F. Optimal performance regions of energy selective electron cooling devices consisting of three reservoirs. Eur Phys J Plus 2019;134:273.
[11] Lee SW, Yang Y, Lee HW, Ghasemi H, Kraemer D, Chen G, et al. An electrochemical system for efficiently harvesting low-grade heat energy. Nat Commun 2014;5:3942.
[12] Gao C, Yin Y, Zheng L, Liu Y, Sim S, He Y, et al. Engineering the electrochemical temperature coefficient for efficient low-grade heat harvesting. Adv Funct Mater 2018;28:1803129.
[13] Liu Y, Gao C, Sim S, Kim M, Lee SW. Lithium manganese oxide in an aqueous electrochemical system for low-grade thermal energy harvesting. Chem Mat 2019;31:4379–84.
[14] Cheng C, Wang S, Tan P, Dai Y, Yu J, Cheng R, et al. Insights into the thermopower of thermally regenerative electrochemical cycle for low grade heat harvesting. ACS Energy Lett 2021;6:329–36.
[15] Zhang H, Zhang F, Yu J, Zhou M, Luo W, Lee YM, et al. Redox targeting-based thermally regenerative electrochemical cycle flow cell for enhanced low-grade heat harnessing. Adv Mater 2021;33:2006234.
[16] Jiang J, Tian H, He X, Zeng Q, Niu Y, Zhou T, et al. A CoHCF system with enhanced energy conversion efficiency for low-grade heat harvesting. J Mater Chem A 2019;7:23862–7.
[17] Yang Y, Loomis J, Ghasemi H, Lee SW, Wang YJ, Cui Y, et al. Membrane-free battery for harvesting low-grade thermal energy. Nano Lett 2014;14:6578–83.
[18] Yang Y, Lee SW, Ghasemi H, Loomis J, Li X, Kraemer D, et al. Charging-free electrochemical system for harvesting low-grade thermal energy. Proc Natl Acad Sci 2014;111:17011–6.
[19] Li X, Li J, Yun J, Wu A, Gao C, Lee SW. Continuous thermally regenerative electrochemical systems for directly converting low-grade heat to electricity. Nano Energy 2022;101:107547.
[20] Wang Y, Cai L, Peng W, Zhou Y, Chen J. Maximal continuous power output and parametric optimum design of an electrochemical system driven by low-grade heat. Energy Convers Manage 2017;138:156–61.
[21] Guo J, Wang Y, Gonzalez-Ayala J, Roco JMM, Medina A, Hernández AC. Continuous power output criteria and optimum operation strategies of an upgraded thermally regenerative electrochemical cycles system. Energy Convers Manage 2019;180:654–64.
[22] Poletayev AD, McKay IS, Chueh WC, Majumdar A. Continuous electrochemical heat engines. Energy Environ Sci 2018;11:2964–71.
[23] Reynard D, Dennison CR, Battistel A, Girault HH. Efficiency improvement of an all-vanadium redox flow battery by harvesting low-grade heat. J Power Sources 2018;390:30–7.
[24] Long R, Li B, Liu Z, Liu W. Multi-objective optimization of a continuous thermally regenerative electrochemical cycle for waste heat recovery. Energy 2015;93:1022–9.
[25] Long R, Li B, Liu Z, Liu W. Performance analysis of a thermally regenerative electrochemical cycle for harvesting waste heat. Energy 2015;87:463–9.
[26] Chen R, Xu W, Deng S, Zhao R, Choi SQ, Zhao L. A contemporary description of the Carnot cycle featured by chemical work from equilibrium: The electrochemical Carnot cycle. Energy 2023;280:128168.
[27] Chen R, Xu W, Deng S, Zhao R, Choi SQ, Zhao L. A comparative study of electrochemical Brayton cycle and thermally regenerative electrochemical cycle. Energy Convers Manage 2023;291:117308.
[28] Long R, Li B, Liu Z, Liu W. A hybrid system using a regenerative electrochemical cycle to harvest waste heat from the proton exchange membrane fuel cell. Energy 2015;93:2079–86.
[29] Al-Nimr MA, Dawahdeh AI, Ali HA. Power generation by integrating a thermally regenerative electrochemical cycle (TREC) with a solar pond and underground heat exchanger. Renew Energy 2022;189:663–75.
[30] Fathabadi H. Improving the power efficiency of a PV power generation system using a proposed electrochemical heat engine embedded in the system. IEEE Trans Power Electron 2019;34:8626–33.
[31] Gerlach DW, Newell TA. Basic modelling of direct electrochemical cooling. Int J Energy Res 2007;31:439–54.
[32] Huang L. Energy and exergy performance comparison of different HFC/R1234yf mixtures in vapor-compression cycles. J Therm Anal Calorim 2020;140:2447–59.
[33] Bai L, Liu S, Ye Z, He M. Investigation on the performance of R1234ze(E) in absorption refrigeration and ejection refrigeration systems. Appl Therm Eng 2019;161:114120.
[34] Lai HM. An enhanced adsorption cycle operated by periodic reversal forced convection. Appl Therm Eng 2000;20:595–617.
[35] Zhao H, Yuan T, Gao J, Wang X, Yan J. Conventional and advanced exergy analysis of parallel and series compression-ejection hybrid refrigeration system for a household refrigerator with R290. Energy 2019;166:845–961.
[36] Bansal PK, Martin A. Comparative study of vapour compression, thermoelectric and absorption refrigerators. Int J Energy Res 2000;24:93–107.
[37] Min G, Rowe DM. Experimental evaluation of prototype thermoelectric domestic-refrigerators. Appl Energy 2006;83:133–52.
[38] Ding Z, Chen L, Sun F. Optimum performance analysis of a combined thermionic-thermoelectric refrigerator with external heat transfer. J Energy Inst 2015;88:169–80.
[39] Zhang Z, Peng Z, Ma Z, Zhang C. Effect of quantum reflection over the barrier on thermionic refrigeration. J Appl Phys 2020;128:044301.
[40] Eriksen D, Engelbrecht K, Bahl CRH, Bjork R, Nielsen KK, Insinga AR, et al. Design and experimental tests of a rotary active magnetic regenerator prototype. Int J Refrig 2015;58:14–21.
[41] Lozano JA, Capovilla MS, Trevizoli PV, Engelbrecht K, Bahl CRH, Barbosa JR. Development of a novel rotary magnetic refrigerator. Int J Refrig 2016;68:187–97.
[42] Abdollahipour A, Sayyaadi H. A review of thermally regenerative electrochemical systems for power generation and refrigeration applications. Appl Therm Eng 2021;187:116576.
[43] Zhang H, Wang Q. Thermally regenerative electrochemical cycle for low-grade heat harnessing. Chem Phys Rev 2021;2:021304.